A Hole-free Shifted Coprime Array for DOA Estimation

Fatimah Abdulnabi Salman[1] and Bayan Mahdi Sabbar[2]

[1]*Al-Nahrain University, Baghdad, Iraq,*
[2]*Al-Mustaqbal University, Baghdad, Iraq*

https://doi.org/10.26636/jtit.2025.1.1959

Abstract — Coprime arrays have recently become a popular trend in estimating the direction of arrival in array signal processing, as they increase the degree of freedom (DOF). Coprime arrays utilize a couple of uniform linear subarrays to create a difference co-array with specific preferable features. In this paper, three proposed structures are considered that depend on the shifting of one of the two uniform linear arrays. The proposed configurations reveal a sequence of lags obtained by filling the holes of the co-array, which span the aperture array. The displacement value depends on the value of the pair of data in the array. The resulting virtual array achieved by means of the proposed methods may generate DOFs *MN* + 1, *MN* + *N* + 1, and *MN* + 2*N* – 2, respectively. The performance of the proposed configurations is evaluated by experimental simulations aiming to demonstrate the effectiveness of the array's design.

Keywords — coprime array, difference co-array, direction of arrival estimation, hole-free array

1. Introduction

Direction of arrival estimation (DOA) is an important topic in array signal processing due to its numerous applications in sonar, wireless communication, radar and navigation [1]–[4] systems. Previously, high-resolution algorithms, such as MUSIC, ESPIRIT, and Root-MUSIC have been proposed to solve the problem of estimating signal direction [5], [6].

These methods are capable of detecting sources with $N-1$ on a uniform linear array with N elements. However, these methods require a large signal-to-noise ratio and numerous snapshots to keep operating properly. In most real cases, the number of snapshots is limited by the operational parameters and physical restrictions that impede efficient DOA estimation [7].

Being able to detect a number of sources that is higher than the number of elements, i.e. increasing the degrees-of-freedom DOFs, has become an interesting topic of research. To cope with this issue, a sparse array structure formed based on a co-array is according to [8], [9], a prospective method capable of increasing DOFs. It attains DOA estimation by locating the sparsest exhibition of the data. A sparse array is composed of two uniform linear subarrays (ULAs).

Distinct sparse arrays, such as the minimum redundancy array (MRA) [10], have been developed to achieve higher DOFs using a limited number of elements. MRA is a sparse array having a maximum number of virtual elements with no holes for the difference co-array, but it lacks general model expression. The DOFs for a certain number of elements cannot be achieved exactly. A nested array [11] may be designed by nesting two ULAs in which the spacing may determine $\mathrm{O}(N2)$ with N elements.

The concept of a co-prime array [12] has attracted the attention of researchers, since co-prime arrays sample the signal sparsely with high resolution and lower cost [2]. The co-prime concept resolves a number of sources that is higher than the number of its elements. Coprime arrays use $M+N-1$ elements to detect $\mathrm{O}(MN)$ sources. Despite a significant number of innovative works relying on the coprime difference co-array, coprime array still suffers from a drawback, as its difference co-array does not provide continuous lags. It has holes that considerably decrease the number of obtainable DOFs.

Several works have focused on proposals to deal with the hole problem. [13] is a good example, where an approach to a coprime array with an extension of one subarray has been proposed. It requires $2M+N-1$ elements to resolve $\mathrm{O}(MN)$ DOFs. The consecutive lags of the difference co-array range are extended with more elements.

The authors of [14] proposed two generalized coprime array configurations with compressed interelement spacing (CACIS) and displaced subarrays (CADiS). For the CACIS configuration, the distance of the elements in the N-subarray is compressed by a compression factor (CF) to keep the minimum distance between the elements, which results in elements overlapping in the self and cross-lag differences. In the CADiS configuration, the N subarray is shifted by a predefined distance to increase the minimum distance between the subarrays in order to expand the aperture size and increase the number of unique lags [14], [15].

However, it breaks the DCA into segments, and critical holes are created that disturb the contiguous lags, which degrades the performance of DOA estimation methods that rely on spatial smoothing.

In article [16], the authors presented extensive research on identifying the location of holes in DCA and proposed two array structures, i.e. the k-times extended coprime array (kECA) and a complementary coprime array (CCA) to fill the holes. In the kECA structure, the M-subarray elements are increased to kM elements to extend the contiguous lags. For the CCA structure, additional elements equal to $M-1$ are

added to fill the holes. The main drawback of the development of these arrays is the extra cost borne due to the presence of additional physical elements.

Furthermore, mutual coupling is affected by the extra element pairs with a small distance present in the kECA structure, and the close element distribution with the distance of half a wavelength in the CCA structure. The authors of [17] proposed a coprime array with suppressed and displaced subarrays (CASDiS) as well as nested displaced coprime subarrays (NesDCoP). For the CASDiS array configuration, the N-subarray is compressed to modify the interelement spacing of the subarray; then, it is shifted by $M + MN$. For the NesDCoP array configuration, the N-subarray is rotated to the negative axis by 180°, compressed by M/CF and then shifted by $N + 1$ to provide hole-free lags.

Article [18] describes a hole-free coprime array (HFCA) developed based on the known number of total elements, in which a maximum number of uDOFs can be achieved by computing the optimal value of M and N.

The problem of holes in coprime arrays may be avoided by redesigning their geometry. In [19], [20] a hole-free array structure is proposed by rearranging the position of the elements in one of the subarrays. The goal is achieved by designing a nested array, with its essentiality property being then analyzed to enhance the array's configuration and extend the aperture array size.

The arrangement of a sparse array in a field affords an adequate but productive manner to plan coprime arrays in order to achieve more lags. Afterwards, only contiguous lags are excluded by means of DOA spatial smoothing estimation techniques, by applying interpolation techniques handling all the lags, or by using sparse array motion. Different coprime configurations, such as generalized coprime and spatial smoothing-MUSIC, have been used in the design process to improve contiguous lags that result in high DOFs.

In this paper, a new array geometry configuration is proposed to improve the available unique lags. A particular emphasis is placed on contiguous lags, and the methods provides a hole-free difference co-array. Thus, spatial efficiency and uniform DOA parameters are exceeded. The array exploits the shifting effects of one coprime array to extend the number of contiguous lags, thus resulting in high DOF. This configuration has resulted in generating hole-free lags.

The paper is structured as follows. Section 2 introduces the fundamental array signal model of coprime arrays, based on difference co-arrays. In Section 3, the proposed array geometry design is presented. The results and conclusions are provided in Sections 4 and 5, respectively.

In this paper, we use upper-case bold characters to represent matrices and lower-case bold characters for vectors. $[\cdot]^T$, $[\cdot]^*$ and $[\cdot]^H$ stand for transpose, the conjugate and conjugate transpose of a vector or matrix, respectively. $\mathrm{Diag}(\cdot)$ and $\mathrm{vec}(\cdot)$ mean a diagonal matrix and the vectorization operator. $\mathrm{E}\{\cdot\}$ represents the expectation operator. I_K indicates a identity matrix with the size of $K \times K$.

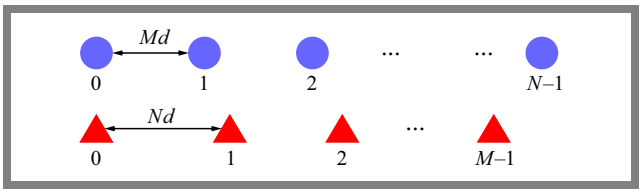

Fig. 1. Configuration of conventional coprime array.

2. Signal Model

The coprime array configuration consists of two ULAs, as illustrated in Fig. 1. N and M are a coprime integer number, such that $N > m$ and $\mathrm{GCD}(M, N) = 1$, where GCD is the largest common divisor, and the two CAs are aligned in a collinear manner. It depends on the concept of the co-array, which refers to the set of points at which the spatial correlation function can be estimated with that array.

The co-array concept has been used in planar design and in estimating the spectrum of multidimensional applications. It may be defined as a set of vectors spacing between points in the elements of given apertures. The vector set is the difference set between the elements or the sum set between array elements of the grid [21]– [23]. The first subarray consists of N sensors with nMd spacing and the second subarray consists of m sensors with mNd spacing. The first element is shared by the two subarrays as a reference element. The total number of sensors that comprise the array is $M + N - 1$.

The elements are positioned at the following locations.

$$\mathbb{P} = \{nMd,\ 0 \leqslant n \leqslant N-1\} \cup \{mNd,\ 0 \leqslant m \leqslant M-1\}\,. \quad (1)$$

$\mathbb{P}$ is a vector that indicates the position of the elements comprising the array $= [p_1, \ldots, p_k]^T$, where $p_i \in \mathbb{P}$, for $i = 1, \ldots, K$.

Considering that D uncorrelated, narrowband, and far-field source signals with power $[\sigma_1^2, \sigma_2^2, \ldots, \sigma_D^2]$, strike the array from angles $\theta = [\theta_1, \theta_2, \ldots, \theta_D]$, the signal received in the array will be declared as:

$$\begin{aligned} x(t) &= \sum_{i}^{D} a(\theta_d)\, S(t) + n(t) \\ &= As(t) + n(t) \in C^{(M+N-1)\times D}\,, \end{aligned} \quad (2)$$

where A is the steering matrix of the style:

$$\begin{aligned} A &= \left[a(\theta_1), a(\theta_2), \ldots, a(\theta_d)\right] \in C^{(M+N-1)\times D} \\ &= \left[1, e^{j\frac{2\pi p_2}{\lambda}\sin(\theta_d)}, \ldots, e^{j\frac{2\pi p_k}{\lambda}\sin(\theta_d)}\right], \end{aligned} \quad (3)$$

$s(t)$ is the signal vector:

$$s(t) = \left[s_1(t), s_2(t), \ldots, s_D(t)\right] \in C^{D\times K}\,, \quad (4)$$

and $n(t)$ is the noise vector:

$$n(t) = \left[n_1(t), n_2(t), \ldots, n_{N+M-1}(t)\right]. \quad (5)$$

The noise is considered independent and distributed randomly with a Gaussian distribution and zero mean invariance. The correlation matrix of the data vector $x(t)$ is collected as:

$$R_{xx} = E\left[x(t)x^H(t)\right] = AR_{SS}A^H = \sigma_n^2 I_{M+N-1}\,, \quad (6)$$

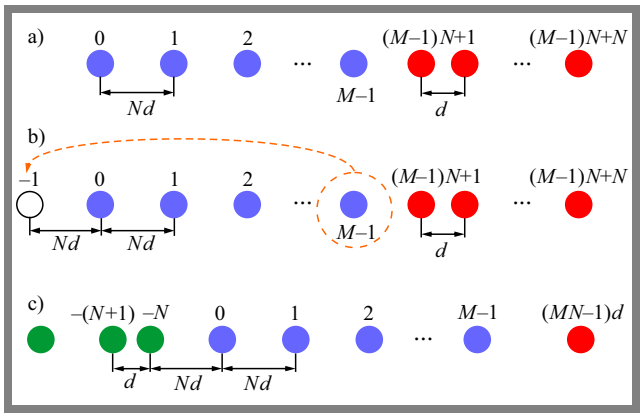

Fig. 2. Hole-free coprime array (FH-CA) configurations for models: a) HF-CA1, b) HF-CA2, and c) HF-CA3.

where $R_{ss} \in C^{D\times D}$ is the source signal covariance matrix and may be expressed as:

$$R_{ss} = \text{diag}\big([\sigma_1^2, \sigma_2^2, \ldots, \sigma_D^2]\big)\,, \in C^{D\times D}. \tag{7}$$

$R_{nn} = \sigma_n^2 I_{M+N-1} \in C^{(M+N-1)\times(M+N-1)}$ is the noise covariance matrix. The covariance matrix is estimated using a limited number of snapshots.

3. Proposed Array Configurations

Three hole-free coprime array (HF-CA) configurations based on PCA on a fixed platform are proposed, as shown in Fig. 2. The first configuration of the HF-CA1 array is illustrated in Fig. 2a. The first subarray consists of M number of elements, while the second subarray consists of N elements. The first subarray elements are positioned at:

$$\mathbb{P}_1 = \big\{0, N, \ldots, (M-1)N\big\}d\,. \tag{8}$$

The second subarray is displaced based on the position of the last sensor in the array, which is $(M-1)N$, and is set as the first sensor location in the new array configuration. The final subarray configuration of the second subarray is as follows:

$$\mathbb{P}_2 = \big\{(M-1)N + n\big\}d, \quad \text{where } 0 \leqslant n \leqslant N\,. \tag{9}$$

The reference element is located at $(M-1)N$, which is shared by the two subarrays, and the total number of the sensor array is $M+N$. The final array geometry for the HF-CA1 array is expressed as:

$$\begin{aligned}\mathbb{P}^{HF-CA1} &= \mathbb{P}_1 \cup \acute{\mathbb{P}}_2 \\ &= \big\{0, N, \ldots, (M-1)N\big\}d \cup \big\{(M-1)N + n\big\}d\,,\end{aligned} \tag{10}$$

where $n = 0, 1, \ldots, N$, the first sensor is located at zero point, and the last sensor is positioned at MN.

$DCA(\mathbb{D})$ of the HF-CA1 array can be illustrated as follows:

$$\begin{aligned}\mathbb{P}^{HF-CA1} &= \big\{(\mathbb{P}_1 - \acute{\mathbb{P}}_2) \cup (\mathbb{P}_1 - \acute{\mathbb{P}}_1) \cup (\mathbb{P}_2 - \acute{\mathbb{P}}_2)\big\} \\ &= \mathbb{D}_{12} \cup \mathbb{D}_{11} \cup \mathbb{D}_{22}\,,\end{aligned} \tag{11}$$

where:

$$\mathbb{D}_{12} = \big\{(mNd - (M-1)Nd + nd), 0 \leqslant m \leqslant M-1, 1 \leqslant n \leqslant N\big\}\,, \tag{12}$$

$$\mathbb{D}_{11} = \big\{mNd,\ \ 0 \leqslant m \leqslant M-1\big\}\,, \tag{13}$$

$$\mathbb{D}_{22} = \big\{\big((M-1)Nd + nd\big) - \big((M-1)Nd + nd\big), 1 \leqslant n \leqslant N\big\}\,. \tag{14}$$

The resulting virtual HF-CA1 array will be a hole-free solution that can be implemented to any M, N pairs. The properties of HF-CA1 can be summarized as follows:

- It contains contiguous lags ranging from $-MN$ to MN, which means that the number of uDOF is $2MN+1$,
- The number of unique lags is $2MN+1$, which is equal to uDOFs, since it is a hole-free array.

To determine the element that has no impact on the DCA, the following relations are considered:

$$\mathbb{D}_{12} \cap \mathbb{D}_{22} = n,\ \ 1 \leqslant n \leqslant N-1\,, \tag{15}$$

$$\mathbb{D}_{12} \cap \mathbb{D}_{11} = mN,\ \ 1 \leqslant m \leqslant M-1\,. \tag{16}$$

From Eq. (15), and considering the relation $\mathbb{D}_{12} \cap \mathbb{D}_{22} \notin \mathbb{P}_1, \acute{\mathbb{P}}_2$, meaning $n \notin \mathbb{P}_1, \acute{\mathbb{P}}_2$, it is easy to observe that the difference of intersection of the self-lags of the difference and cross-lags difference does not represent the position of any element in the actual elements of the matrix. Therefore, it cannot be considered for determining the non-essential element in the array configuration.

From Eq. (16), one may see that the intersecting elements are part of the actual array (M-subarray) that needs to be considered. To determine which element does not contribute to the DCA, the following preposition is presented.

Let

$$\begin{aligned}\mathbb{D}_3 &= \{\acute{\mathbb{P}}_2 - mNd,\ \ 1 \leqslant m \leqslant M-1\} \\ &= (M-1)Nd + nd - mNd,\ \ \text{for } m = M-1, \\ \mathbb{D}_3 &= (M-1)N + n - (M-1)N = n\,.\end{aligned}$$

It has been shown in the previous relation in Eq. (16) that $n \notin \mathbb{P}_1, \acute{\mathbb{P}}_2$, so the element at position $(M-1)N$ does not affect the resulting virtual array. For $m \leqslant M-1, \mathbb{D}_3 \neq n$, so removing any elements from that set may result in a virtual array with holes.

To create an example illustrating the essential importance of the position of elements, M and N are set to 5 and 6, respectively. According to Eqs. (1)–(3), the elements are positioned at $\mathbb{P} = \{0, 6, 12, 18, 24\}d \cup \{25, 26, 27, 28, 29, 30\}d$. Figure 3a shows the configuration of the HF-CA1 array and its difference co-array, where the DCA is a hole-free array, while Fig. 3b-e shows the arrays and their DCAs when one element is removed.

One may notice that the DCA presented in Fig. 3e is similar to the one from Fig. 3a. Therefore, the element at position $(M-1)N = 24$ is not an essential element and does not affect DCA.

After removing the non-essential element from the array configuration, the DCA($\mathbb{D}$) can be expressed in the following manner:

$$\acute{\mathbb{D}} = \acute{\mathbb{D}}_{12} \cup \acute{\mathbb{D}}_{11} \cup \mathbb{D}_{22}\,, \tag{17}$$

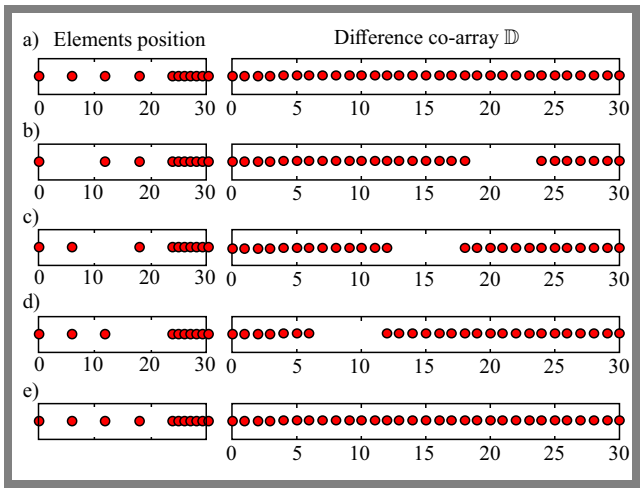

Fig. 3. HF-CA1 configuration and its DCA a), essentiality testing after removing an element from M-subarray at 6 b), 12 c), 18 d), and 24 e), respectively.

where:

$$\begin{aligned}\acute{\mathbb{D}}_{12} &= \big\{(mNd-(M-1)Nd+nd),\\ &\quad 0\leqslant m\leqslant M-2,\ \ 1\leqslant n\leqslant N\big\}\\ \mathbb{D}_{11} &= \big\{mNd,\ \ 0\leqslant m\leqslant M-2\big\}\,.\end{aligned} \tag{18}$$

The configuration of the HF-CA2 array depends on identifying the non-essential element in the HF-CA1 array. The HF-CA2 array is illustrated in Fig. 2b. In this configuration, the nonessential element at position $(M-1)Nd$ is moved to the $-Nd$ location. To justify the new location of the moved elements, the following consideration is presented.

Let us $\delta = \min(\acute{\mathbb{P}}_2) - \max(\acute{\mathbb{P}}_2)$. The reason for selecting $\acute{\mathbb{P}}_2$ is that its self-difference provides a consecutive number with the unit distance between the elements. Regarding the relation given in Eq. (17), the new position of the element may be obtained as follows:

$$\delta = \big\{(M-1)N+\min(n)\big\} - \big\{(M-1)N+\max(n)\big\} = -N\,. \tag{19}$$

The location of the elements in HF-CA2 can be expressed as follows:

$$\mathbb{P}^{HF-CA2} = \mathbb{P}_1 \cup \acute{\mathbb{P}}_2 \cup \mathbb{P}_3\,, \tag{20}$$

where:

$$\mathbb{P}_1 = \big\{mNd,\ \ 0\leqslant m\leqslant (M-1)N\big\}\,, \tag{21}$$

$$\acute{\mathbb{P}}_2 = \big\{(M-1)N+n\big\}d\,, \tag{22}$$

$$\mathbb{P}_3 = -Nd\,. \tag{23}$$

This configuration will reduce the redundancy rate and increase the number of uDOFs. The properties of the HF-CA2 array can be summarized as follows:

- it contains contiguous lags ranging from $MN-N$ to $MN+N$, which means the number of uDOFs is $2MN+2N+1$. The number of uDOFs in the HF-CA2 array is increased by N.
- the number of unique lags is $2MN+2N+1$, since it is a hole-free array, the number of unique lags is equal to the number of uDOFs.

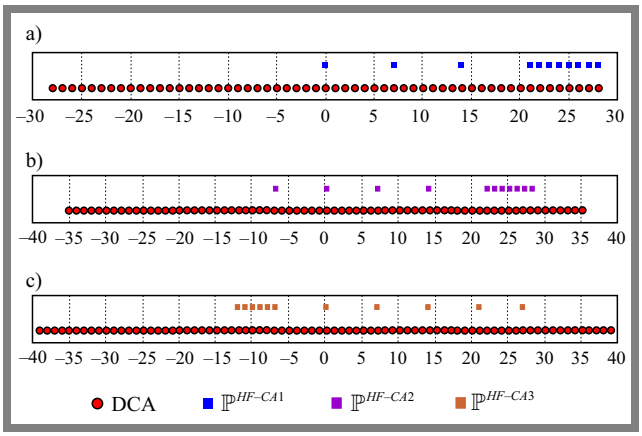

Fig. 4. Example of the HF-CA configuration when $M=4$ and $N=7$ for: a) HF-CA1, b) HF-CA2, and c) HF-CA3.

To achieve more DOFs with particularly contiguous lags, the HF-CA3 configuration is proposed by rotating the dense N-subarray by 180° along the negative side, then the last element in the N-subarray is relocated to the $MN-1$ position, as demonstrated in Fig. 2c. The following relation expresses the position of elements in HF-CA3:

$$\mathbb{P}^{HF-CA3} = \mathbb{P}_1 \cup \mathbb{P}_2 \cup \mathbb{P}_3\,, \tag{24}$$

where:

$$\mathbb{P}_1 = \big\{mNd,\ \ 0\geqslant m\geqslant (M-1)N\big\}\,, \tag{25}$$

$$\mathbb{P}_2 = \big\{-(N:2N-2)\big\}d\,, \tag{26}$$

$$\mathbb{P}_3 = (MN-1)d\,. \tag{27}$$

The idea behind the HF-CA3 configuration is presented below. The subarrays with the location set:
$\mathbb{P}_1$ and $\mathbb{P}_2 = \{-(N:2N-1)\}d$, i.e. the rotated N-subarray, form a hole-free virtual array ranging from $-MN-N+1$ to $MN+N-1$ which is less than the HF-CA2 configuration. If the last element in $\mathbb{P}_2$ is removed, the DCA will have holes located at positions $(mN+N-1)d,\ \ 0\leqslant m\leqslant M-1$. To fill the holes and extend the DCA, the removed element is positioned at $(MN-1)d$, which represents the location of the last element in the hole set.

The properties of the HF-CA3 array can be summarized as follows:

- It contains contiguous lags ranging from $-MN-2N+3$ to $MN+2N-3$, meaning the number of uDOFs is $2MN+4N-5$. The number of uDOFs in the HF-CA3 array is increased by $N-3$.
- The number of unique lags is $2MN+4N-5$, since it is a hole-free array, the number of unique lags is equal to the number of uDOFs.

For illustration, an example is shown in Fig. 4 for the HF-CA configuration with $M=4$ and $N=7$. This is the deployment of the location of the actual elements and the

Tab. 1. Comparison of the closed-form expression for HF-CA1, HF-CA2, and HF-CA3 array configurations with other array types.

Array type	Aperture size	Consecutive lags	Total number of elements
HF-CA1	$MN+1$	$2MN+1$	$M+N$
HF-CA2	$MN+N+1$	$2MN+2N+1$	$M+N$
HF-CA3	$MN+2N-2$	$2MN+4N-5$	$M+N$
Ma-HFCA [18]	$3M+N(K+1-N-\frac{M}{2})-1$	$2N(K+1-N-\frac{N}{2})+6M-1$	K
CADSiS [17]	$2MN+M$	$4MN+1$	$2M+N$
NesDCoP [17]	$2MN+N$	$4MN+2N+1$	$2M+N$
CCA [16]	$kMN-N$	$2kMN-2N+1$	$(k+1)M+N-2$
k-times [16]	$kMN-N$	$2(k-1)MN+2M-1$	$kM+N-1$
ECA [13]	$2MN-N$	$2MN+2M-1$	$2M+N-1$

DCA of the three HF-CA configurations. One may notice that all the HF-CA configurations are hole-free arrays. HF-CA1 is capable of generating a ULA segment within the $[-28:0:28]$ range, while HF-CA2 and HF-CA3 may generate ULA segments within the $[-35:0:35]$ and $[-39:0:39]$ ranges, respectively. HF-CA3 can achieve the largest uDOF with an extension to the array aperture size, which makes it capable of identifying more sources.

Table 1 shows the comparison of the closed form expressions of the lags generated by HF-CA1, HF-CA2, and HF-CA3 array configurations, with different coprime array types, depending on the array aperture size, contiguous lags and the total number of elements.

4. Simulation Results

The proposed HF-CA designs were tested using Matlab to verify the weight function, array robustness, spatial spectrum, and RMSE. The weight function $w(m)$ of the M,N pair, $m \in D$ is the number of elements pairs that have the same value in the DCA index m. The weight function $w(m)$ of the ULA having M,N elements meets the following characteristics [15]:

$$w(0)=(M,N), \sum_{m\in D} w(m)=(M,N)^2, w(m)=w(-m)\ . \tag{28}$$

The weight function gives an indication of the element allocation in an array. The weight functions $w(m)$ show different distributions of the virtual array elements. A smaller weight function means that there are fewer pairs with one partition that is who getting a sparse array structure. As the weight function is minimized, the root means square error (RMSE) is decreased as well [24].

Figure 5 illustrates the weight function, worked out according to Eq. (28), of the proposed array designs with different array types, such as PCA, ECA, CACIS, CADiS, k-times ECA, CCA, CASDiS, NesDCoP, and Ma-HFCA with 9 elements. In the figure, the blue dots represent the positions of the physical elements, while the red dots represent the virtual lags and the red crosses represent the locations of holes. One may notice that PCA, ECA, k-times ECA, CACIS, and CADiS cannot provide a hole-free sparse array and the range for their ULA segment is $[-9:0:9]$, $[-14:0:14]$, $[-14:0:14]$, $[-16:0:16]$, and $[8:23,-8:-23]$, respectively.

The remaining array structures provide a hole-free co-array with an ULA segment. The consecutive sets are: $[-15:0:15]$, $[-20:0:20]$, $[-25:0:25]$, $[-23:0:23]$, $[-20:0:20]$, $[-25:0:25]$ and $[-27:0:27]$ for CCA, CASDiS, NesDCoP, Ma-HFCA, HF-CA1, HF-CA2, and HF-CA3, respectively.

It can be seen that the proposed HF-CA3 outperforms its rivals, as it has the highest number of consecutive lags compared to other array types. Another remark regarding the ULA segments for CASDiS, HF-CA1 and NesDCoP, HF-CA2 for 9 elements is that these array designs can have the same ranges of consecutive lags. This is not always true for other numbers of the elements, as can be seen from Tab. 2.

Considering the weight functions related to Eq. (28), as shown in Fig. 5, $w(1)$ for CADiS is zero, since there is no element in the first position (there is a hole). $w(1)=2$ for PCA, ECA, k-times ECA and CASIC. $w(1)=3$ for CCA, Ma-HFCA and HF-CA3. $w(1)=4$ for CADiS, NesDCoP and HF-CA2. $w(1)=5$ for CASDiS and HF-CA2, while $w(2)=2$ for PCA, ECA, k-times ECA, Ma-HFCA and HF-CA3. $w(2)=3$ for NesDCoP and HF-CA2. $w(2)=4$ for CADiS, CASDiS and HF-CA1, and $w(2)=5$ for CCA and CACIS.

4.1. Evaluation of Robustness

Various array structures are evaluated based on their resistance to failure. In the exercise, the location of the antenna may lead to some disturbance, including the antenna's failure in some radical situations. Several parameters are used to evaluate robustness, including spatial efficiency and redundancy rate.

Spatial efficiency is the ratio between the number of contiguous lags and the length of the virtual array aperture for the positive side in a sparse array [25].

Tab. 2. Comparison of different array types against aperture, number of DOFs, and operational robustness.

Array type	M, N pairs	Number of elements	Array aperture	Number of uDOFs	Spatial efficiency	Redundancy rate
ECA [13]	(3, 4)	9	20	29	69.23%	56.79%
k-times [16]	$K = 2$, (3, 4)	9	20	29	69.23%	56.79%
CCA [16]	$K = 2$, (2, 5)	9	15	31	100%	66.12%
NA [9]	(4, 5)	9	25	51	100%	39.50%
CACIS [14]	(4, 5)	9	21	33	79.48%	54.32%
CADiS [14]	(4, 5)	9	27	16	74.20%	44.44%
CASDiS [17]	(2, 5)	9	19	39	100%	61.00%
NesDCoP [17]	(2,5)	9	25	51	100%	37.04%
Ma-HFCA [18]	(2, 3)	9	23	47	100%	42.00%
HF-CA1	(4, 5)	9	20	41	100%	49.40%
HF-CA2	(4, 5)	9	25	51	100%	37.04%
HF-CA3	(4, 5)	9	27	55	100%	32.10%
ECA [13]	(3, 8)	13	40	53	64.55%	60.35%
k-times [16]	(6, 7)	13	48	97	100%	42.60%
CCA [16]	(5, 9)	13	40	53	79.48%	54.32%
NA [9]	(6, 7)	13	50	30	60%	44.44%
CACIS [14]	$K = 3$, (3, 4)	13	40	65	79.74%	56.80%
CADiS [14]	$K = 2$, (3, 5)	13	25	51	100%	64.58%
CASDiS [17]	(4, 5)	13	44	81	90.80%	49.70%
NesDCoP [17]	(4, 5)	13	45	91	100%	41.42%
Ma-HFCA [18]	(3, 5)	13	48	97	100%	42.60%
HF-CA1	(6, 7)	13	42	85	100%	49.70%
HF-CA2	(6, 7)	13	49	99	100%	41.42%
HF-CA3	(6, 7)	13	53	107	100%	36.68%

$$\eta = \frac{\text{Number of uDoFs}}{\text{Array aperture size}} . \tag{29}$$

Spatial efficiency has an impact on signal determination and estimation efficiency. Higher spatial efficiency of the coprime virtual array structure may ensure high DOA estimation performance, meaning fewer waste elements in the DCA.

Table 2 shows the spatial efficiency for five different types of arrays. It can be noted that the proposed HF-CA array configuration ensures 100% spatial efficiency, when compared with the remaining types. The HF-CA array designs provide contiguous lag with a hole-free array configuration, which is equal to the unique lags.

The lagged redundancy rate is the measure of repeated spatial lag for pairs of elements in an array. It can be defined as [16]:

$$r_{redun} = \frac{|\mathbb{P}|^2 - |\mathbb{D}|}{|\mathbb{P}|^2} \tag{30}$$

where set $\mathbb{P}$ represents the positions of the physical array elements and set $\mathbb{D}$ stands for DCA.

Although the redundancy rate can reverberate robustness to some extent, it suffers from some constrictions. When redundancy is limited to specific levels, high levels of robustness cannot be obtained even though there is a high redundancy rate. From Fig. 5, one may notice that the highest level of redundancy is centered on the zeroth element position, and it is equal to the number of the physical elements in the sparse array structure. It can be noted that CADiS and the second proposed array configuration have no positions without any redundancy.

The DOA estimates of spatial spectrum of the proposed array structures are shown in Fig. 6.

The array configuration is based on $M = 4, N = 5$, so the total number of elements in the array is 9. The simulation parameters are set to 10 dB, the number of snapshots is 500, and the source angle is θ_i uniformly distributed within the range $-60°, \ldots, 60°$. For the HF-CA1 structure, the number of sources is set to $Q = 18$. The design of the HF-CA1 matrix can generate 41 DOFs within the $[20 : 0 : 20]$ range. From Fig. 6a, one may notice that the HF-CA1 array can estimate

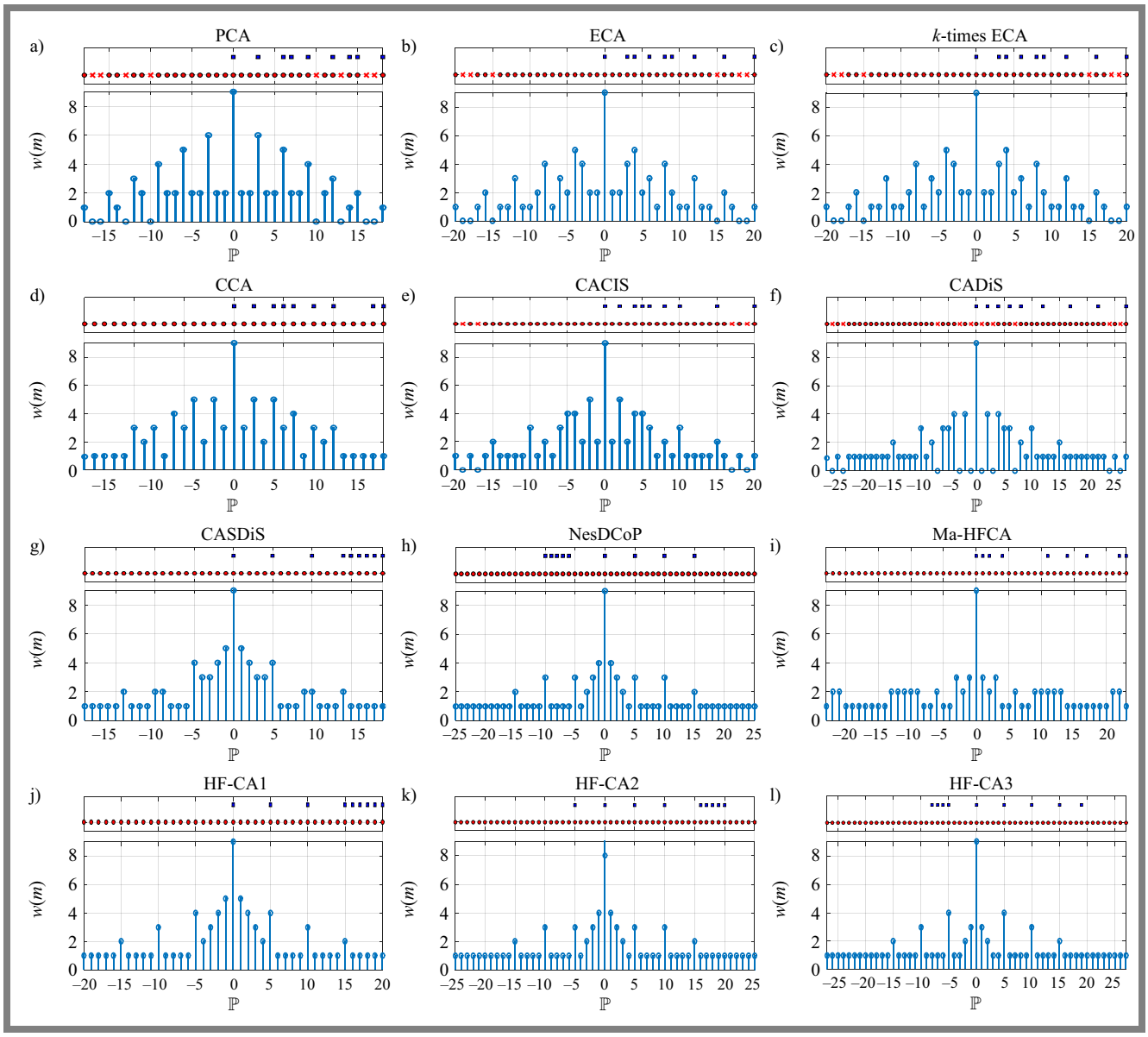

Fig. 5. Weight function for different array configurations.

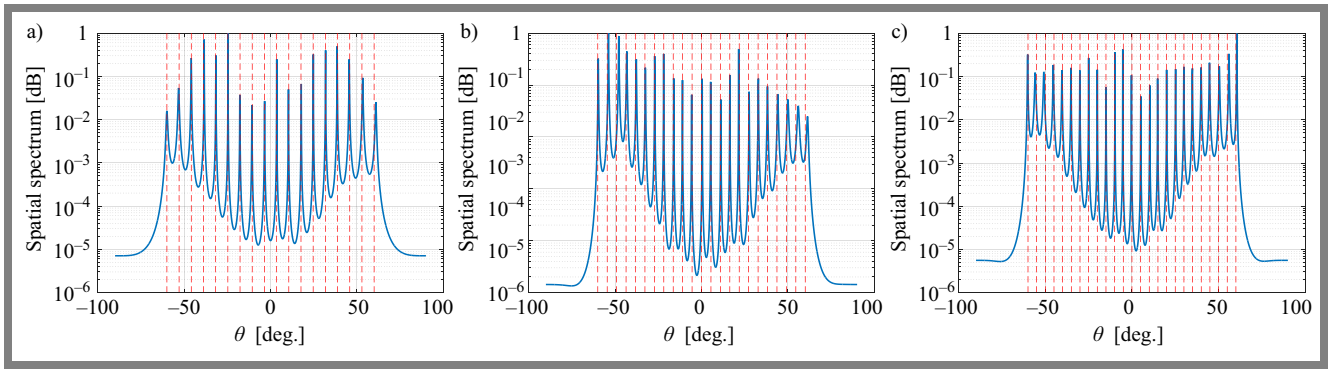

Fig. 6. Spatial spectrum estimation ($\{textSNR = 10\ dB$ and snapshot $= 500$) for: a) HF-CA1 with $Q = 18$, b) HF-CA2 with $Q = 23$, and HF-CA3 with $Q = 25$.

18 sources effectively. For the HF-CA2 structure, the number of sources is set to $Q = 23$. The HF-CA2 array design can generate 51 DOFs within the $[-25 : 0 : 25]$ range. It can resolve the 23 sources accurately, as shown in Fig. 6b. For HF-CA3, the number of sources is set to $Q = 25$ and all the sources can be resolved correctly as shown in Fig. 6c,

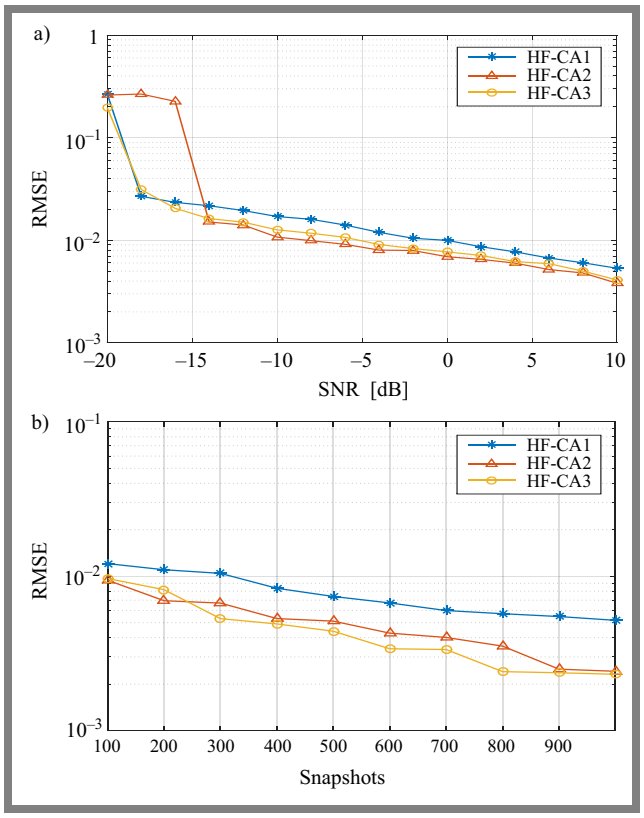

Fig. 7. RMSE evaluation for HF-CA for: a) snapshots $= 500$ and $D = 12$ sources and b) SNR $= 0$ and $D = 12$ sources.

since HF-CA3 can generate a uniform segment within the $[-27 : 0 : 27]$ range and the number of DOFs is 55.

4.2. RMSE Evaluation

The root mean square error (RMSE) is one of the most common metrics that is used to evaluate the accuracy of DOA estimation. Calculations of the error between the true and estimated DOA are given in [26]–[27]:

$$RMSE = \sqrt{\frac{1}{QM_C}\sum_{i=1}^{M_C}\sum_{q=1}^{Q}(\tilde{\theta}_{q(i)} - \theta_q)^2}\,, \qquad (31)$$

where M_C denotes the number of total Monte Carlo trials, Q is the number of sources and $\tilde{\theta}_{q(i)}$ are the true and estimated DOA, respectively.

The RMSE vs. SNR ratio is shown in Fig. 7a. It can be seen that HF-CA2 and HF-CA3 configurations outperform the HF-CA1 array configuration, because there are more DOFs used for DOA estimation. Figure 7b illustrates the RMSE vs. snapshots ratio. HF-CA2 and HF-CA3 methods outperform the HF-CA1 configuration as the number of snapshots increases.

5. Conclusions

In this paper, hole-free coprime array structures are proposed with the positions of their elements being shifted and moved from one location to another. These proposed methods can achieve a higher number of contiguous lags and a hole-free array structure, when compared with other structures. The performance of the array structure was evaluated using different robustness parameters, such as spatial efficiency and redundancy rate, in addition to aperture size and number of DOFs, and a comparison with other array structures was performed. The results of simulations and numerical analyses revealed the effectiveness of the proposed methods.

References

[1] H. Krim and M. Viberg, "Two Decades of Array Signal Processing Research: The Parametric Approach", *IEEE Signal Processing Magazine*, vol. 13, no. 4, pp. 67–64, 1996 (https://doi.org/10.1109/79.526899).

[2] Z. Weng and P.M. Djuric, "A Search-free DOA Estimation Algorithm for Coprime Arrays", *Digital Signal Processing*, vol. 24, pp. 27–33, 2014 (https://doi.org/10.1016/j.dsp.2013.10.005).

[3] F.A. Salman and B.M. Sabbar, "DOA Estimation Exploiting Moving Platform of Unfolded Coprime Array", *International Journal of Intelligent Engineering and Systems*, vol. 15, no. 2, pp. 532–542, 2022 (https://doi.org/10.22266/ijies2022.0430.47).

[4] F.A. Salman and B.M. Sabbar, "Estimation of Coherent Signal on Modified Coprime Array", *16th International Middle Eastern Simulation and Modelling Conference*, 2020.

[5] R. Schmidt, "Multiple Emitter Location and Signal Parameter Estimation", *IEEE Transaction Antenna Propagation*, vol. 34, no. 3, pp. 276–280, 1986 (https://doi.org/10.1109/TAP.1986.1143830).

[6] R. Roy and T. Kailath, "ESPRIT – Estimation of Signal Parameters via Rotational Invariance Technique", *IEEE Transactions Acoustics, Speech, and Signal Processing*, vol. 37, no. 7, pp. 984–995, 1989 (https://doi.org/10.1109/29.32276).

[7] W. Baxter and E. Aboutanios, "Fast Direction of Arrival Estimation in Coprime Arrays", *International Conference on Radar (RADAR)*, Brisbane, Australia, 2018 (https://doi.org/10.1109/RADAR.2018.8557304).

[8] X. Wang, X. Wang, and X. Lin, "Co-prime Array Processing with Sum and Difference Co-array", *49th Asilomar Conference on Signals, Systems and Computers*, Pacific Grove, USA, 2015 (https://doi.org/10.1109/ACSSC.2015.7421152).

[9] X. Wang, Z. Chen, S. Ren, and S. Cao, "DOA Estimation Based on the Difference and Sum Co-array for Coprime Arrays", *Digital Signal Processing*, vol. 69, pp. 22–31, 2017 (https://doi.org/10.1016/j.dsp.2017.06.013).

[10] A.T. Moffet, "Minimum-redundancy Linear Arrays", *IEEE Transactions on Antennas and Propagation*, vol. 16, no. 2, pp. 172–175, 1968 (https://doi.org/10.1109/TAP.1968.1139138).

[11] P. Pal and P.P. Vaidyanathan, "Nested Arrays: A Novel Approach to Array Processing with Enhanced Degrees of Freedom", *IEEE Transactions on Signal Processing*, vol. 58, no. 8, pp. 4167–4181, 2010 (https://doi.org/10.1109/TSP.2010.2049264).

[12] P.P. Vaidyanathan and P. Pal, "Sparse Sensing with Co-prime Samplers and Arrays", *IEEE Transactions on Signal Processing*, vol. 59, no. 2, pp. 573–586, 2011 (https://doi.org/10.1109/TSP.2010.2089682).

[13] P. Pal and P.P. Vaidyanathan, "Coprime Sampling and the Music Algorithm", *Digital Signal Processing and Signal Processing Education Meeting (DSP/SPE)*, Sedona, USA, 2011 (https://doi.org/10.1109/DSP-SPE.2011.5739227).

[14] S. Qin, Y.D. Zhang, and M.D. Amin, "Generalized Coprime Array Configuration for Direction of Arrival Estimation", *IEEE Transactions on Signal Processing*, vol. 63, no. 6, pp. 1377–1390, 2015 (https://doi.org/10.1109/TSP.2015.2393838).

[15] A. Raza, W. Liu, and Q. Shen, "Thinned Coprime Arrays for DOA Estimation", *25th European Signal Processing Conference (EUSIPCO)*, Kos, Greece, 2017 (https://doi.org/10.23919/EUSIPCO.2017.8081236).

[16] X. Wang and X. Wang, "Hole Identification and Filling in K-times Extended Co-prime Arrays for Highly-efficient DOA Estimation", *IEEE Transactions on Signal Processing*, vol. 67, no. 10, pp. 2693–2706, 2019 (https://doi.org/10.1109/TSP.2019.2899292).

[17] K. Shabir, T.H. Al Mahmud, R. Zheng, and Z. Ye, "Generalized Super-resolution DOA Estimation Array Configurations' Design Exploiting Sparsity in Coprime Arrays", *Circuits Systems and Signal Processing*, vol. 38, pp. 4723–4738, 2019 (https://doi.org/10.1007/s00034-019-01078-1).

[18] P. Ma, J. Li, F. Xu, and X. Zhang, "Hole-free Coprime Array for DOA Estimation: Augmented Uniform Co-array", *IEEE Signal Processing Letters*, vol. 28, pp. 36–40, 2021 (https://doi.org/10.1109/LSP.2020.3044019)

[19] F.A. Salman and B.M. Sabbar, "Semi-symmetrical Coprime Linear Array with Reduced Mutual Coupling Effect and High Degrees of Freedom", *International Journal of Computing and Digital Systems*, vol. 15, no. 1, pp. 1483–1495, 2024 (https://iiict.uob.edu.bh/IJCDS/papers/IJCDS1501105_1570871127.pdf).

[20] F.A. Salman and B.M. Sabbar, "Initial Phase Effect on Direction Finding Using Coprime Array", *International Middle Eastern Simulation and Modelling Conference*, Baghdad, Iraq, 2022.

[21] D.A. Linebarger, I.H. Sudborough, and I.G. Tollis, "Difference Bases and Sparse Sensor Arrays", *IEEE Transactions on Information Theory*, vol. 29, no. 2, pp. 716–721, 1993 (https://doi.org/10.1109/18.212309).

[22] J.H. McClellan, "Multidimensional Spectral Estimation", *Proceedings of the IEEE*, vol. 70, no. 9, pp. 1029–1039, 1982 (https://doi.org/10.1109/PROC.1982.12431).

[23] S.W. Lang and J.H. McClellan, "Spectral Estimation for Sensor Arrays", *IEEE Transactions on Acoustics, Speech, and Signal Processing*, vol. 31, no. 2, pp. 349–358, 1983 (https://doi.org/10.1109/TASSP.1983.1164080).

[24] C.-L. Liu and P.P. Vaidyanathan, "Super Nested Arrays: Linear Sparse Arrays with Reduced Mutual Coupling – part 1: Fundamentals", *IEEE Transactions on Signal Processing*, vol. 64, no. 15, pp. 3997–4012, 2016 (https://doi.org/10.1109/TSP.2016.2558159).

[25] Y.D. Zhang, S. Qin, and M.G. Amin, "DOA Estimation Exploiting Coprime Arrays with a Sparse Sensor Spacing", *IEEE International Conference on Acoustic, Speech, and Signal Processing*, Florence, Italy, 2014 (https://doi.org/10.1109/ICASSP.2014.6854003).

[26] G. Qin, M.G. Amin, and Y.D. Zhang, "DOA estimation exploiting sparse array motions", *IEEE Transactions on Signal Processing*, vol. 67, no. 11, pp. 3013–3027, 2019 (https://doi.org/10.1109/TSP.2019.2911261).

[27] F.A. Salman and B.M. Sabbar, "Low-complexity DOA Estimation Method Based on Joined Coprime Array", *Journal of Telecommunications and Information Technology*, no. 1, pp. 11–16, 2024 (https://doi.org/10.26636/jtit.2024.1.1350).

Fatimah Abdulnabi Salman, Ph.D.
System Engineering Department
https://orcid.org/0000-0001-8875-9844
E-mail: faty_salman@nahrainuniv.edu.iq
Al-Nahrain University, Baghdad, Iraq
https://nahrainuniv.edu.iq

Bayan Mahdi Sabbar, Prof.
Medical Instrumentation Techniques Engineering Department
https://orcid.org/0000-0003-0541-2410
E-mail: prof.dr.bayan.mahdi@uomus.edu.iq
Al-Mustaqbal University, Baghdad, Iraq
https://uomus.edu.iq